Canadian Science Publishing | Canadian Journal of Earth Sciences

Ordovician mafic magmatism in an Ediacaran arc complex, Sibak, NE Iran: the eastern tip of the Rheic Ocean

Journal:	*Canadian Journal of Earth Sciences*
Manuscript ID	cjes-2018-0072.R1
Manuscript Type:	Article
Date Submitted by the Author:	31-May-2018
Complete List of Authors:	Moghadam, Fereshteh; Shahid Beheshti University, 19839-63113 Tehran, Masoudi, Fariborz; Shahid Beheshti University Faculty of Earth Sciences Corfu, Fernando; Department of Geosciences, Homam, Seyed ; Ferdowsi University of Mashhad Department of Geology
Keyword:	granite, gabbro, Ediacaran, Ordovician, Rheic Ocean
Is the invited manuscript for consideration in a Special Issue? :	Not applicable (regular submission)

Ordovician mafic magmatism in an Ediacaran arc complex, Sibak, NE Iran: the eastern tip of the Rheic Ocean

F. Ranjbar Moghadam[1], F. Masoudi[1], F. Corfu[2], and S.M. Homam[3]

[1]Shahid Beheshti University, Faculty of Earth Sciences, 19839-63113 Tehran, Iran

[2]University of Oslo, Department of Geosciences and CEED, Oslo, Norway

[3]Ferdowsi University of Mashhad, Faculty of Science, Mashhad, Iran,

Corresponding author:

Fernando Corfu, University of Oslo, Department of Geosciences and CEED

Postbox 1047 Blindern, N-0316 Oslo NORWAY

fernando.corfu@geo.uio.no

Tel: (+47) 22 85 66 80, Fax: (+47) 22 85 42 15

other e-mail addresses:

Fereshteh Moghadam fereshtehmoghadam@yahoo.com

Fariborz Masoudi drfmasoudi@yahoo.com

Seyed Massoud Homam homam@um.ac.ir

Abstract: The assembly of Gondwana in the Ediacaran was concluded by extensive arc magmatism along its northern margin. Extensional events in the Early Paleozoic led to rifting and the eventual separation of terranes which were later assimilated in different continents and orogens. The Sibak area of northeastern Iran records these events, including Late Precambrian volcanic-sedimentary processes, metamorphism, and magmatism. A granite at Chahak in the Sibak Complex yields a zircon U-Pb age of 548.3 ± 1.1 Ma whereas a spatially associated gabbro has an age of 471.1 ± 0.9 Ma. The latter corresponds to the earliest stages of rifting in the nearby Alborz domain with the deposition of clastic sedimentary sequences, basaltic volcanism, and, as indicated by indirect evidence, coeval granitic plutonism. The Chahak gabbro is thus one of earliest witnesses of the rifting processes which eventually led to the development of the Rheic Ocean, and were indirectly linked to subduction of Iapetus at the Laurentian margin and the early development of the Appalachian orogen.

Keywords: Granite, Gabbro, Ediacaran, Ordovician, Rheic Ocean

Introduction

Gondwana reached its major extension in the late Precambrian through the amalgamation of several cratons and accretion by arc magmatism, especially along its northern margin (e.g., Cawood and Buchan 2007). In the Early Paleozoic arc accretion was followed by the gradual separation of ribbon terranes and the opening of new oceanic basins (Fig. 1A; Stampfli and Borel 2002; Neubauer 2002; Nance et al. 2010; Domeier and Torsvik 2014; von Raumer et al. 2015; Domeier 2017). In the west, the Avalonian terranes drifted off, opening the large Rheic (Ran) Ocean, and eventually accreting to Baltica and Laurentia in a complex succession of events including the Taconic, Salinic, Acadian and Neoacadian orogenies (e.g. van Staal et al. 2009, 2012; Nance et al. 2010; Macdonald et al. 2017). Opening of the Paleotethys in the Devonian (Stampfli et al. 2013) corresponds to the major separation of the Variscan terranes (also referred to as Cadomian or as the Hun superterrane of Stampfli and Borel 2002), which now are dispersed through most of central and western Europe (Neubauer 2002; Torsvik and Cox 2013; von Raumer et al. 2015). The exact identity and timing of development of the various Paleozoic seaways at the border of the main Panthalassa Ocean, however, remain poorly defined and different names have been variously used for the same geographic features (Rheic, Ran, Proto-Tethys, Paleotethys, Palaeo-Asian oceans). The Early Paleozoic extensional processes also affected the central and eastern margins of Gondwana, but the exact mechanisms and the extent of the separation remain speculative. In detail the plate aggregation and splitting processes were complex reflecting the variable interactions of subduction, convergence and divergence.

Our study is focused on a metamorphic complex in northeastern Iran that records the final stages of growth of the Gondwanan margin at the Precambrian-Cambrian boundary and the emplacement of Ordovician gabbros, which herald the transition to the extensional processes mentioned above.

Geological setting

The Central Iranian Terrane (Ramezani and Tucker 2003) is a collage of three major crustal domains: the Lut, Tabas and Yazd blocks (Fig. 1B). They are composed of crust formed mainly between 600 and 520 Ma by arc magmatism (e.g. Ramezani and Tucker 2003; Hassanzadeh et al. 2008; Shafaii Moghadam et al.

2015*a*, 2017*a*). Arc magmatism was followed by the development of a stable passive margin with epicontinental shelf sedimentation including evaporite and carbonate deposits, shallow-water arkosic sandstones and shales, and eventually marine carbonates (Berberian and King 1981; Alavi 1996). Extensional processes are recorded in the Ordovician, and especially in the Silurian, in the eastern Alborz zone by rift-related clastic sedimentary rocks and basaltic magmatism (Ghavidel-syooki and Winchester-Seeto 2002; Derakhshi and Ghasemi 2015). The crust was subsequently affected by a number of events including Carboniferous rifting processes and formation of oceanic crust (Shafaii Moghadam et al. 2015*b*), Permian-Triassic closing of the Paleotethys, followed by a sequence of Mesozoic and Cenozoic magmatic and tectonic stages recording subduction of oceanic crust during closing of the Neotethys and collision with the Arabic plate (Stöcklin 1968; Berberian and King 1981; Sengör et al. 1988; Sengör 1990; Stampfli et al. 1991; Bagheri and Stampfli 2008; Fard and Davydov 2015).

The study area (Fig. 1C) in the northeast of Iran is situated at the edge of the Lut block in the Central Iranian Terrane. It comprises an amphibolite facies metamorphic succession, the metavolcanic and sedimentary Sibak Complex, a metamorphosed dolomite (Soltanieh), and granitic and gabbroic rocks (de Gramont et al. 1984). The general trend of the rocks is NW-SE and the contacts are mainly faulted. These basement units are locally covered by the Jurassic Shemshak Formation, a molasse-type unit deposited at the end of the Cimmerian orogeny, by Early Cretaceous orbitolina limestone with interlayers of dark shale, Late Cretaceous sandstone, conglomerate and limestone, Paleocene and Eocene volcanic rocks with marl, sandstone, gypsum and conglomerate and Miocene clastic sedimentary rocks (de Gramont et al. 1984).

The basal Neoproterozoic metapelitic units are exposed in a narrow elongated belt which widens to the north-west. The most complete section of the metamorphic series can be observed in the northwestern corner of the 1/100000 scale Kariz Now geological map (de Gramont et al. 1984). These units are composed of a thick series of micaschists, characterized by the presence of large crystals of andalusite and/or sillimanite, cordierite and garnet formed at the upper limit of the amphibolite facies under low pressure - high temperature regional metamorphic conditions (Ranjbar 2010). Although there are are no direct age constraints the geological relationships suggest that metamorphism occurred in the latest Ediacaran. Horizons of highly recrystallized limestone interlayered with micaschist, and small lenses of pegmatites with large crystals of tourmaline are locally present in the metamorphic series. Gneissose rocks are the other variety of the series, mainly of a quartz-feldspathic nature. Sheared gneisses are lighter in color and finer grained than mica schists.

The Sibak Complex comprises metavolcanic rocks, schists and marble (de Gramont et al. 1984). The contact between the Sibak Complex and andalusite mica schist of the metapelitic unit is faulted. The complex is also in faulted contact with the granitic and gabbroic intrusions and with the Soltanieh recrystallized dolomites farther south. A NW-SE trending, subvertical, post-overthrusting fault system separates the Sibak complex and andalusite schists from the uplifted dolomitic unit.

Granitic and gabbroic intrusions are widespread and show sharp faulted contacts to metavolcanic rocks, schists and metasandstones of the Sibak Complex and to the adjacent recrystallized dolomites. According to de Gramont et al. (1984) the Sibak Complex comprises granitic to quartz-dioritic bodies of irregular shape and extent, commonly with a gneissose, blastomylonitic texture, and difficult to separate from the enclosing rocks, with which they frequently form migmatite-like associations. The most continuous outcrop of intrusives is located in the south-eastern part of the complex. One granitic body of very restricted extent is observed to cut across the dolomite unit in the northwestern part of the map. The main granite occurrence near Chahak is an irregular body, about 15 km long and maximum 1 km wide (Fig. 2A). Partovifar (2012) described the granitic rocks as medium potassic calc-alkaline I-type whereas Ranjbar (2010) considered the granitic rocks as S-type. A zircon U-Pb age of 630-650 Ma is mentioned in de Gramont et al. (1984), but the data are not published. In light of our new results reported below it is likely that this date, likely still obtained using large mg-size bulk fractions, is too old because the analysis included some inherited zircon grains, also seen in our work.

Metagabbros to quartz-diorites appear next to the main granitic intrusion as small bodies with similar color and morphology as rocks units in the Sibak Complex, making it difficult to map the outcrops (Fig. 2B). The contacts between gabbro and granite are also faulted, but Homam (2015) concluded that gabbros are younger than the granite.

Petrography

<u>Metapelites</u>

This unit is dominated by andalusite mica schists, characterized by the presence of large andalusite porphyroblasts. Three different mineralogical assemblages can be distinguished, from the north towards the south of the study area (abbreviations after Kretz 1983).

1: Qtz + Bt + Pl + Ms + And + Crd + Grt.

2: Qtz + Pl + Bt + Ms + And + Sil ± Grt ± Crd.

3: Qtz + Pl + Bt + Ms + Kfs + And + Sil ± Grt ± Crd.

Cordierite porphyroblasts show rounded shapes with sector twinning and are mostly replaced, completely or partially, by micaceous aggregates. Andalusite porphyroblasts are either poikiloblastic with no well-formed crystal faces or idioblastic chiastolite. Garnet crystals vary in size and show idioblastic to xenoblastic forms. Sillimanite is common as fibrolitic intergrowths in biotite, muscovite and plagioclase, as needles and as long prisms growing from the groundmass. Larger sillimanite crystals form by coarsening of fibrolite radiating out from quartz and feldspar grain boundaries. In the third assemblage there are also coarse perthitic K-feldspar crystals with inclusions of biotite, quartz and muscovite.

<u>Sibak Complex</u>

The metavolcanic rocks in the Sibak Complex include metarhyolite, porphyritic andesite and intermediate and mafic tuffite. Metamorphic conditions range from lower greenschist to amphibolites facies.

The felsic metavolcanic rocks are hololeucocratic in hand specimen. Deformed grains of quartz, with undulose extinction and locally recrystallization to a microgranoblastic texture, occur besides embayed quartz phenocrysts and slightly sericitized K-feldspars. Zoned and variously sericitized plagioclase phenocrysts have deformed twinning lamellae and are partly recrystallized. Biotite, epidote, iron oxide and carbonate minerals are also present in the rhyolites and with additional hornblende in the dacites. The accessory minerals are zircon, epidote and iron oxides.

Meta-andesites are fine grained and variously porphyritic rocks. The phenocrysts include plagioclase, pyroxene and biotite with accessory epidote, clinozoisite and iron oxide in a groundmass of sericitic plagioclase and glass. Myrmekitic textures are present. Most pyroxene phenocrysts have been replaced by hornblende, and secondary carbonate is also observed.

Tuffitic rocks are mainly green and generally strongly altered. They mostly consist of volcanic rock fragments, with amphibole, secondary chlorite and carbonate. Based on the size of lithic fragments the rock classifies as lapilli tuff.

<u>Chahak granite</u>

The granite is a light pink, medium grained rock, frequently gneissose or blastomylonitic (Fig. 2A). It exhibits a hypidiomorphic granular texture and consists of quartz, sodic plagioclase, biotite, epidote, chlorite, hornblende and accessory iron oxide, zircon, titanite, apatite and calcite. The most common mineral is medium to coarse grained quartz with subidiomorphic to anhedral shapes. Some quartz crystals have undulose extinction as an effect of the progressive deformation, and locally exhibit chessboard extinction, subgrain and new grain deformation lamellae The K-feldspar occurs as large perthitic microcline porphyroclasts and exhibits some argillic alteration. Zoning and different degrees of sericitization and saussuritization are observed in the plagioclase, which is sodic and has deformed twinning lamellae (Fig. 2D). In some samples a myrmekitic texture is also present. Biotite flakes are variously chloritized. Rare hornblende crystals are present but muscovite is absent.

<u>Gabbro</u>

In the study area, the original gabbro has been dynamically metamorphosed to amphibolite gabbro. The rock is medium- to fine-grained and is composed of plagioclase, pyroxene, hornblende, biotite, and olivine as major minerals and apatite, ilmenite and magnetite as minor minerals. The most dominant texture is hypidiomorphic granular, but intergranular and porphyric textures are also present. Plagioclase (oligoclase) occurs as subhedral to euhedral crystals ranging in size from 0.1 to 0.6 mm and showing sericitic alteration. Euhedral to subhedral phenocrysts of diopside comprise 15-20% of the rock (Fig. 2C). Primary hornblende occurs as dark brown and deep green subhedral crystals. Some amphiboles show rhythmic overgrowths which represent deep-seated crystallization in volatile-rich magma under conditions of high but varying gas pressure (Homam 2015). Secondary pale green actinolite is present, in part pseudomorphing pyroxen or as overgrowths on hornblende containing a core of exsolved pyroxene. In most of the examples, hornblende and biotite also form corona textures around plagioclase, pyroxene and olivine, while plagioclase, pyroxene and olivine show obvious corrosion features. These relationships most probably reflect reactions of early formed crystals with aqueous fluid or evolved melt and/ or solid-state fluid-enhanced metamorphic reactions.

Geochemistry

Four samples of the granite were selected from outcrops close to Chahak village (Fig. 1C) for chemical analysis (1-F,2-F, 3-F, 4-F). Chemical data for the gabbro have been reported previously (Homam 2015) but their main characteristics are discussed below. The samples were prepared at Shahid Beheshti University, Teheran. Fresh rock chips were powdered to 75 μm using a tungsten carbide ball mill, dried in an oven at 100 ^{o}C, and kept in a desiccator before analysis. Major element oxides were determined with X-ray fluorescence (XRF) and an inductively coupled plasma emission spectrometer (ICP-MS (MA250) was used for trace elements in same samples. The latter analyses were carried out by Bureau Veritas Mineral Laboratories, Vancouver (Canada).

The chemical analyses for the granite are reported in table 1. The SiO_2 content ranges from 69 to 71 wt.% and in the classification diagram of De la Roche et al. (1980, not shown) the data plot in the fields of granite to granodiorite. The samples are calc-alkaline and peraluminous, with ASI [molar Al_2O_3/($CaO + K_2O + Na_2O$)] ranging from 1 to 1.1.

In the spider diagram (Fig. 3B) the Chahak granite samples reveal an enrichment in large ion lithophile elements (LILEs), negative anomalies for Nb and Ta, positive spikes at Pb, Zr and Y and a negative one at Sr. The REE patterns (Fig. 3A) are characterized by a fractionation between light and heavy REEs and an absent or weak negative Eu anomaly. In the diagrams of Y+Nb vs. Rb and Y vs. Nb (Fig. 4) the granites show an arc affinity.

Chemical analyses of the gabbro are reported in Homam (2015) and are also plotted in Fig. 3, for comparison with the granite data. The samples exhibit SiO_2 contents ranging from 49 to 52 wt.%. In the spider diagram the data show enrichment in the LILE, but no or only very weak negative Nb-Ta anomalies. There are small positive anomalies for Sr and Y, and a major positive anomaly for Pb. The REE show a moderate fractionation with a weak positive Eu anomaly. Homam (2015) shows that the gabbros are tholeiitic and he displays a number of trace element plots suggesting an island arc affinity of the magmas.

U-Pb geochronology

Analytical technique

The analyses were carried out by the ID-TIMS U-Pb technique (Krogh 1973). Zircon was separated by crushing, pulverizing, Wilfley table, magnetic separation and heavy liquids. Suitable grains were subjected to either air abrasion (Krogh 1982) or chemical abrasion (Mattinson 2005). The grains were dissolved in HF at 195°C, after addition of a mixed ^{202}Pb-^{205}Pb-^{235}U spike, and processed through ion exchange resin separation and solid source mass spectrometry. Details are described in Corfu (2004). The data are calculated with the decay constants of Jaffey et al. (1971) and plot with the program of Ludwig (2009).

Granite (sample G3-F)

The zircon population consists of euhedral, prismatic or equant crystals, with strongly developed {100} and {101} crystal faces (Fig. 2E). They are mostly clear, but with inclusions of other minerals and melt. The analyses show some scatter that reflects the combination of inheritance and slight Pb loss (Table 2, Fig. 5). Inheritance is evident mainly in one short zircon prism. By contrast, a fraction of long prisms yields a concordant analysis with a concordia age of 548.3 ± 1.1 Ma. The other two analyses are broadly consistent with it, but show some slight deviations interpreted to reflect small amounts of inheritance and Pb loss. The age of 548.3 ± 1.1 Ma is considered the best estimate for crystallization of the granite.

Gabbro

The gabbro yielded just few zircon grains, mostly fragments with few preserved crystal faces. The grains are generally turbid and metamict, but with some domains of more clear and transparent zircon (Fig. 2F). Air abrasion liberated some of these domains of good quality zircon, and two analyses yield concordant and overlapping data giving a Concordia age of 471.1 ± 0.9 Ma (Fig. 5, Table 2). The overall morphology of the population and the variations in U content and degree of metamictization are fairly common in zircon of gabbroic rocks, and thus support an indigeneous origin of the grains. The age is therefore interpreted to date magmatic formation of the gabbro.

Discussion

Geochemical affinity

The granites in the Sibak Complex are mostly peraluminous, calc-alkaline, and with low levels of Ni, MgO, V and Cr (Table 1). Their geochemical features are compatible with an origin by arc magmatism (Fig. 3), which is also supported by the presence of the mafic minerals biotite and hornblende. The presence of xenocrystic zircon, however, implies a certain degree of crustal contamination.

The gabbro has fractionated REE and also relatively elevated LILE. It lacks distinct Nb-Ta negative anomalies, but Homam (2015) presents diagrams such as Y vs. Cr where the data are clearly indicative of an arc affinity. Plots of other elements given in Homan (2015) are, however, more ambiguous on the tectonic affinity.

Neoproterozoic arc magmatism and Ordovician rifting

The Chahak granite intruded at 548.3 ± 1.1 Ma and corresponds thus to an intensive period of Cadomian arc magmatism recorded throughout the Central Iranian Terrane and the other fragments of the original Gondwanan active margin (Ramezani and Tucker 2003; Hassanzadeh et al. 2008; Badr et al. 2013; Bagherzadeh et al. 2015; Shafaii Moghadam et al. 2015*a*). The granite intrudes the volcanic – metasedimentary Sibak Complex, which likely formed in earlier magmatic stages of the arc. The metamorphism of the andalusite – sillimanite mica schists that reached upper amphibolite facies conditions was not directly dated, but the migmatite-like interlayering of schists and granite described by de Gramont et al. (1984), and the lack of contact metamorphism, imply that peak metamorphism and intrusion of the granite were likely essentially coeval.

The more interesting result of the study is the discovery of Mid Ordovician gabbro (471.1 ± 0.9 Ma) in the Sibak Complex. The geochemical features presented by Homam (2015) and discussed above show that the gabbro has some magmatic arc affinity, which would suggest a protracted end of the subduction processes along the northern Gondwanan margin. The alternative is that the specific signature of the mafic magma simply reflects that of a previously metasomatized mantle source (e.g. Murphy et al. 2008). A comparison of the gabbro's geochemical features with those reported by Derakhshi and Ghasemi (2015) for the Late Ordovician-Silurian Soltan Maidan basalts, 400-1200 m thick, in the rift zone north of our field area shows many similarities between the two sets, most notably comparable abundances for SiO_2, Na_2O and K_2O, similar REE patterns with moderate fractionation and lack of significant Eu anomalies. There are also similarities in some trace elements, for example in a Zr/Y vs. Zr diagram (Pearce and Norry 1979) both data sets plot in the field of 'within plate basalt'. Derakhshi and Ghasemi (2015) show that the volcanism was in part submarine and in part subaerial as indicated by the occurrence of pillow basalts and columnar jointing, respectively. They conclude that the Soltan Maidan volcanic rocks are transitional to mildly alkaline and were derived from an enriched mantle source in a rifting and crustal thinning environment.The time of intrusion of the gabbro in the Sibak Complex at 471 Ma corresponds to a precocious stage in these processes of extension recorded immediately to the north by rifting, clastic sedimentation and eruption of basalt; these processes reached their most intense level of activity in the Silurian (Alavi 1996; Ghavidel-Syooki and Winchester-Seeto 2002; Ghaviden-Syooki et al. 2011; Ghobadi Pour et al. 2011; Derakhshi and Ghasemi 2015). The early basalts were examined by Shahri (2008) in the vicinity of Shahrood. He deduced an extensional setting with deposition of turbidite facies sedimentary rocks and initially the eruption of sporadic basaltic flows with intraplate characteristics. There are thus analogies between the basalts in the E-W trending rift and the gabbro emplaced in the outer flank of the rift. A U-Pb study of detrital zircon in sedimentary rocks of the Ordovician Qelli Formation in the Alborz reported abundant Mid Ordovician grains, which along with the Mid-Ordovician granitic clasts in conglomerates of the region attest to the importance of Mid Ordovician magmatism during these extensional events (Shafaii Moghadam et al. 2017*b*).

Paleogeographic implications

This Ordovician magmatism is the expression of complex extensional processes, in part associated with arc magmatism and collision, which have been described for many terranes derived from the northern margin of Gondwana (Fig.

1A; e.g., Valverde-Vaquero and Dunning 2000; Trombetta et al. 2004; Okay et al. 2008*a,b*; Nance et al. 2008). These terranes belong broadly to three families which separated from Gondwana and accreted to other continents at different times: the Avalonian terranes, which separated in the Late Cambrian to Early Ordovician, the Variscan terranes in the Devonian, and the Turkish and Central Iranian terranes in the Triassic-Jurassic.

The Late Cambrian to Early Ordovician separation of the Avalonian terranes opened the Rheic Ocean which expanded at a fast rate, a process linked to slab pull (Nance et al. 2010). This activity was simultaneous with, and preseumably related to subduction of the Iapetus oceanic crust at the Laurentian margin where it resulted in the extensive development of ophiolites and arc sequences, associated with accretionary tectonics (e.g. van Staal et al. 2009, 2012). Segments of this Early Paleozoic Laurentian margin were eventually transferred to the British and Scandinavian Caledonides (e.g. Dunning and Pedersen 1987; Pedersen et al. 1992; Chew and Strachan 2014).

The mechanisms responsible for the Early Paleozoic extensional processes at the Gondwanan margin are not always evident. Neubauer (2002) suggests development of back arcs and eventual separations, based mainly on a consideration of Cambrian activity in the Variscan terranes now embedded in the Alpine Orogen. Murphy et al. (2006) argued that previous sutures controlled the pattern of separation, the Avalonian terranes representing more juvenile crust than the Variscan terranes. Although they did not drift away from Gondwana until later, the evidence for Early Paleozoic extensional activity is well documented in the two youngest groups of terranes, as we demonstrate in this paper for northeast Iran. Extension was locally followed by Ordovician compressional phases and development of unconformities attributed to arc accretion and collision (von Raumer et al. 2015). In the NE-Iranian segment of the Gondwanan margin, however, there is no evidence for Ordovician or Silurian compressional stages.

The rift widened, and in the Devonian it developed into a full oceanic basin, the Paleotethys branch of the Rheic Ocean. It is at this stage that the Variscan terranes driften away from Gondwana. They eventually accreted to Laurussia and the remaining parts of the Paleotethys closed in the Triassic (Stampfli and Borel 2002). The third period of rifting at the Gondwana margin opened up the Neotethys starting in the Triassic, detaching, among others, the Central Iranian Terrane from Gondwana.

Conclusions

The Late Precambrian Sibak Complex and associated mica-schist and dolomite were metamorphosed and intruded by granite at 548.3 ± 1.1 Ma. This event reflects the intense arc magmatism affecting the northern margin of Gondwana. Gabbro spatially associated to the granite intruded later, in the Middle Ordovician at 471.1 ± 0.9 Ma. This event was related to initial rifting along the Alborz region evolving with clastic sedimentation and increasing emplacement of basaltic volcanic rocks. On the larger scale of the northern Gondwanan margin these events fit into a pattern of general extension, locally related to arc and back-arc development, eventually leading to the separation of ribbon microcontinents and coinciding with the opening of the Rheic Ocean. The processes were thus geodynamically linked to subduction of Iapetus oceanic crust at the Laurentian margin and the early development of the Applachian orogen.

Acknowledgements

We thank Brendan Murphy for his constructive review and appreciate suggestions by editor Ali Polat.

References

Alavi, M. 1996. Tectonostratigraphic synthesis and structural style of the Alborz mountain system in northern Iran. Journal of Geodynamics, **21**: 1–33.

Badr, M.J., Collins, A.S., Masoudi, F., Cox, G., and Mohajjel, M. 2013. The U-Pb age, geochemistry and tectonic significance of granitoids in the Soursat Complex, Northwest Iran. Turkish Journal of Earth Science, **22**: 1-31, © TÜBİTAK doi:10.3906/yer-1001-37

Bagheri, S., and Stampfli, G.M. 2008. The Anarak, Jandagh and Posht-e-Badam metamorphic complexes in central Iran: New geological data, relationships and tectonic implications. Tectonophysics, **451**: 123-155.

Bagherzadeh, R.M., Karimpour, M.H., Farmer, G.L., Stern, C.R., Santos, J.F., Rahimi, B., and Shahri, M.R.H. 2015. U–Pb zircon geochronology, petrochemical and Sr–Nd isotopic characteristic of Late Neoproterozoic granitoid of the Bornaward Complex (Bardaskan-NE Iran). Journal of Asian Earth Sciences, **111**: 54-71.

Berberian, M., and King, G.C.P. 1981. Towards a paleogeography and tectonic evolution of Iran. Canadian Journal of Earth Science, **8**: 210–265.

Cawood, P.A., and Buchan, C. 2007. Linking accretionary orogenesis with supercontinent assembly. Earth-Science Reviews, **82**: 217–256.

Chew, D.M. and Strachan, R.A, 2014. The Laurentian Caledonides of Scotland and Ireland. *In* New Perspectives on the Caledonides of Scandinavia and Related Areas. *Edited by* Corfu, F., Gasser, D. and Chew, D.M. Geological Society of London, Special Publications No. 390, pp. 45-91, doi 10.1144/SP390.16

Corfu, F. 2004. U-Pb age, setting and tectonic significance of the Anorthosite-Mangerite-Charnockite-Granite Suite, Lofoten-Vesterålen, Norway. Journal of Petrology, **45**: 1799-1819. doi: 10.1093/petrology/egh034.

de Gramont X.B., Guillou Y., Maurizot, P.,Vaslet, D., and de la Villeon, H. 1984. Geological map of Kariznow. Geological Survey of Iran. Scale 1/100000, sheet 8060.

De la Roche, H., Leterrier, J., Grandclaude, P., and Marchal, M. 1980. A classification of volcanic and plutonic rocks using R1,R2-diagrams and major element analysis—its relationships with current nomenclature, Chemical Geology, **29**: 183–210.

Derakhshi, M., and Ghasemi, H. 2015. Soltan Maidan Complex (SMC) in the eastern Alborz structural zone, northern Iran: magmatic evidence for Paleotethys development. Arabiam Journal of Geosciences, **8**: 849–866, DOI 10.1007/s12517-013-1180-2

Domeier, M. 2016. A plate tectonic scenario for the Iapetus and Rheic Oceans. Gondwana Research, 36: **275**-295.

Domeier, M. 2017. Early Paleozoic tectonics of Asia: Towards a full-plate model. Geoscience Frontiers, **9**: 789-862.

Domeier, M., and Torsvik, T.H. 2014. Plate tectonics in the late Paleozoic. Geoscience Frontiers, **5**: 303-350.

Dunning, G.R. and Pedersen, R.B. 1987. U/Pb ages of ophiolites and arc-related plutons of the Norwegian Caledonides: Implications for development of Iapeus. Contributions to Mineralogy and Petrology, **98**:13-23.

Fard, S.A., and Davydov, V.I. 2015. New Permian Aliyak and Kariz Now formations, Alborz Basin, NE Iran: correlation with the Zagros Mountains and Oman. Geological Journal, **50**: 811–826.

Ghavidel-Syooki, M., and Winchester-Seeto, T. 2002. Biostratigraphy and palaeogeography of Late Ordovician chitinozoans from the northeastern Alborz Range, Iran. Review of Palaeobotany and Palynology, **118**: 77–99.

Ghavidel-Syooki, M., Hassanzadeh, J., and Vecoli, M. 2011. Palynology and isotope geochronology of the Upper Ordovician–Silurian successions (Ghelli and Soltan Maidan Formations) in the Khoshyeilagh area, Eastern Alborz Range, Northern Iran; stratigraphic and palaeogeographic implications. Review of Palaeobotany and Palynology, **164**: 251–271.

Ghobadi Pour, M., Kebriaee-Zadeh, M.R., and Popov, L.E. 2011. Early Ordovician (Tremadocian) brachiopods from the Eastern Alborz Mountains, Iran. Estonian Journal of Earth Sciences, **60**: 65-82. doi: 10.3176/earth.2011.2.01

Hassanzadeh, J., Stockli. D.F., Horton, B.K., Axen, G.J., Stockli, L.D., Grove, M., Schmitt, A.K., and Walker, J.D. 2008. U-Pb zircon geochronology of late Neoproterozoic-early Cambrian granitoids in Iran: Implications for paleogeography, magmatism, and exhumation history of Iranian basement.Tectonophysics, **451**: 71-96.

Homam, M. 2015. Petrology and geochemistry of late Proterozoic hornblende gabbros from southeat of Fariman. Khorasan Razavi province, Iran. Journal of Economic Geology, **7**: 91-111.

Jaffey, A.H., Flynn, K.F., Glendenin, L.E., Bentley, W.C., and Essling, A.M. 1971: Precision measurement of half-lives and specific activities of ^{235}U and ^{238}U. Physical Review, **C4**: 1889-1906.

Kretz, R. 1983. Symbols for rock-forming minerals. American Mineralogist, **68**: 277-279.

Krogh, T.E. 1973. A low-contamination method for hydrothermal decomposition of zircon and extraction of U and Pb for isotopic age determinations. Geochimica et Cosmochimica Acta, **37**: 485-494. doi.org/10.1016/0016-7037(73)90213-5.

Krogh, T.E. 1982. Improved accuracy of U-Pb zircon ages by the creation of more concordant systems using an air abrasion technique. Geochimica et Cosmochimica Acta, **46**: 637-649.

Ludwig, K.R. 2009. Isoplot 4.1. A geochronological toolkit for Microsoft Excel. Berkeley Geochronology Centre Special Publications, No. 4, p. 76.

Macdonald, F.A., Karabinos, P.M., Crowley, J.L., Hodgin, E.B., Crockford, P.W., and Delano, J.W. 2017. Bridging the gap between the foreland and the hinterland II: Geochronology and tectonic setting of Ordovician magmatism and basin formation on the Laurentian margin of New England and Newfoundland: American Journal of Science, **317**: 555-596. doi.org/10.2475/05.2017.02

Mattinson, J.M. 2005. Zircon U-Pb chemical abrasion ("CA-TIMS") method: Combined annealing and multi-step partial dissolution analysis for improved precision and accuracy of zircon ages. Chemical Geology, **220**: 47-66. doi.org/10.1016/j.chemgeo.2005.03.011.

Murphy, J.B., Gutierrez-Alonso, G., Nance, R.D., Fernandez-Suarez, J., Keppie, J.D., Quesada, C., Strachan, R.A., and Dostal, J. 2006. Origin of the Rheic Ocean: rifting along a Neoproterozoic suture? Geology, **34**: 325–328.

Murphy, J.B., Dostal, J., and Keppie, J.D. 2008. Neoproterozoic-Early Devonian magmatism in the Antigonish Highlands, Avalon terrane, Nova Scotia: Tracking the evolution of the mantle and crustal sources during the evolution of the Rheic Ocean. Tectonophysics, **461**: 181–201.

Nance, R.D., Murphy, J.B., Strachan, R.A., Keppie, J.D., Gutiérrez-Alonso, G., Fernández- Suárez, J., Quesada, C., Linnemann, U., D'Lemos, R., Pisarevsky, S.A. 2008. Neoproterozoic–early Paleozoic tectonostratigraphy and palaeogeography of the peri-Gondwanan terranes: Amazonian v. West African connection. *In* The boundaries of the West African Craton. *Edited by* N. Ennih and J.-P. Liégeois. Geological Society of London, Special Publication No. 297, pp. 345–383.

Nance, R.D., Gutiérrez-Alonso, G., Keppie, J.D., Linnemann, U., Murphy, J.B., Quesada, C., Strachan R.A., and Woodcock, N.H. 2010. Evolution of the Rheic Ocean. Gondwana Research, **17**: 194–222.

Neubauer, F. 2002. Evolution of late Neoproterozoic to early Paleozoic tectonic elements in Central and Southeast European Alpine mountain belts: review and synthesis. Tectonophysics, **352**: 87–103.

Okay, A.I., Bozkurt, E., Satır, M., Yiğitbaş, E., Crowley, Q.G., and Shang, C.K. 2008*a*. Defining the southern margin of Avalonia in the Pontides: Geochronological data from the Late Proterozoic and Ordovician granitoids from NW Turkey. Tectonophysics, **461**: 252–264. doi:10.1016/j.tecto.2008.02.004

Okay, A.L., Satir, M., and Shang, C.K., 2008*b*. Ordovician metagranitoid from the Anatolide-Tauride Block, northwest Turkey: geodynamic implications. Terra Nova, **20**: 280–288, doi: 10.1111/j.1365-3121.

Partovifar, F. 2012. Petrology and geochemistry studies of granitic rocks from Chahak village. Kariznow area, southeast of Fariman, Iran. M.Sc thesis, Ferdowsi University, Mashhad, Iran, 145 pp.

Pearce, J.A., and Norry, M.J. 1979. Petrogenetic implications of Ti, Zr, Yand Nb variations in volcanic rocks. Contributions to Mineralogy and Petrology, **69**: 33–47.

Pearce, J.A., Harris, N.B.W., and Tindle, A.G. 1984.Trace element discrimination diagrams for the tectonic interpretation of granitic rocks. Journal of Petrology, **25**: 956-983.

Pedersen, R.B., Bruton, D.L. and Furnes, H. 1992. Ordovician faunas, island arcs and ophiolites in the Scandinavian Caledonides. Terra Nova, **4**: 217-222.

Ramezani, J., and Tucker, R.D. 2003. The Saghand Region, Central Iran: U-Pb Geochronology, Petrogenesis and Implications for Gondwana Tectonics. American Journal of Science, **303**: 622-665, doi.org/10.2475/ajs.303.7.622

Ranjbar, F. 2010. Petrology and petrogenesis of metamorphic rocks of east and southeast of Ghandab. M.Sc thesis. Ferdowsi University, Mashhad, Iran.

Sengör, A.M.C., 1990. A new model for the late Palaeozoic - Mesozoic tectonic evolution of Iran and implicationtions for Oman. *In* The Geology and Tectonics of the Oman region. *Edited by* A.H.F. Robertson, M.P. Searle and A.C. Ries. Geological Society of London, Special Publication No. 49, pp. 797-831.

Sengör, A.M.C., Altiner, D., Cin, A., Ustaömer, T., and Hsü, K.J. 1988. Origin and assembly of Tethyside orogenic collage at the expense of Gondwana Land. *In* Gondwana and Tethys. *Edited by* M.G Audley-Charles and A. Hallam. Geological Society of London, Special Publication No. 37, pp. 119-181.

Shafaii Moghadam, H., Khademi, M., Hu, Z., Stern, R.J., Santos, J.F., Wu, Y. 2015*a*. Cadomian (Ediacaran–Cambrian) arc magmatism in the ChahJam–Biarjmand metamorphic complex (Iran): Magmatism along the northern active margin of Gondwana. Gondwana Research, **27**: 439–452.

Shafaii Moghadam, H.S., Li, X.-H., Ling, X.-X., Stern, R.J., Khedr, M.Z., Chiaradia, M., Ghorbani, G., Arai, S., Tamura, A., 2015*b*. Devonian to Permian evolution of the Paleo-Tethys Ocean: new evidence from U–Pb zircon dating and Sr–Nd–Pb isotopes of the Darrehanjir–Mashhad "ophiolites", NE Iran. Gondwana Research, **28**: 781–799.

Shafaii Moghadam, H., Li, X.-H., Santos, J.F., Stern, R.J.,Griffin, W.L., Ghorbani, G., Sarebani, N. 2017*a*. Neoproterozoic magmatic flare-up along the N. margin of Gondwana: The Taknar complex, NE Iran. Earth and Planetary Science Letters, **474**: 83–96.

Shafaii Moghadam, H., Li, X.-H., Griffin, W.L., Stern, R.J, Thomsen, T.B., Meinhold, G., Aharipour, R., and O'Reilly, S.Y. 2017*b*. Early Paleozoic tectonic reconstruction of Iran: Tales from detrital zircon geochronology. Lithos, **268–271**: 87–101.

Shahri, H.M. 2008. Pre-rifting evidence of Paleotethys in the southwest of Shahrood, northeastern Iran. World Applied Sciences Journal, **3**: 154-161, Stampfli, G.M. and Borel, G.D. 2002. A plate tectonic model for the Paleozoic and Mesozoic constrained by dynamic plate boundaries and restored synthetic oceanic isochrons. Earth and Planetary Science Letters, **196**: 17-33.

Stampfli, G.M., Marcoux, J., and Baud, A. 1991. Tethyan margins in space and time. Palaeogeography, Palaeoclimatology, Palaeoecology, **87**: 373-409.

Stampfli, G.M., Hochard, C., Vérard, C., Wilhem, C., and von Raumer, J. 2013. The formation of Pangea. Tectonophysics, **593**: 1-19.

Stöcklin, J., 1968. Structural history and tectonics of Iran: a review. American Association of Petroleum Geologists Bulletin, **52**: 1229–1258.

Sun, S.-S., and McDonough, W.F. 1989. Chemical and isotopic systematic of oceanic basalts: implications for mantle composition and processes. *In* Magmatism in the Ocean Basins. *Edited by* A.D. Saunders and M.J. Norry. Geological Society of London, Special Publications No. 42, pp. 313-345.

Torsvik, T.H. and Cocks, L.R.M. 2013. Gondwana from top to base in space and time. Gondwana Research, **24**: 999-1030.

Trombetta, A., Cirrincione, R., Corfu, F., Mazzoleni, P., and Pezzino, A. 2004. Mid-Ordovician U-Pb ages of porphyroids in the Peloritan Mountains (NE Sicily): palaeogeographic implications for the evolution of the Alboran microplate. Journal of the Geological Society, London, **161**: 265-276.

Valverde-Vaquero, P., and Dunning, G.R. 2000. New U–Pb ages for early Ordovician magmatism in central Spain. Journal of the Geological Society of London, **157**: 15–26.

van Staal, C.R., Whalen, J.B., Valverde-Vaquero, P., Zagorevski, A., and Rogers, N. 2009. Pre-Carboniferous, episodic accretion-related, orogenesis along the Laurentian margin of the northern Appalachians. *In* Ancient orogens and modern analogues *Edited by* Murphy, J.B., et al., Geological Society of London, Special Publications No. 327, pp. 271–316.

Van Staal, C.R., Barr, S.M., and Murphy, J.B. 2012. Provenance and tectonic evolution of Ganderia: constraints on the evolution of the Iapetus and Rheic oceans. Geology, **40**: 987-990.

von Raumer, J.F., Stampfli, G.M, Arenas, R., and Sánchez Martínez, S. 2015. Ediacaran to Cambrian oceanic rocks of the Gondwana margin and their tectonic interpretation. Internation Journal of Earth Sciences, **104**: 1107–1121. doi 10.1007/s00531-015-1142-x

Figure captions

Fig. 1. (**A**) Paleogeographic plate model at 470 Ma showing the general situation along the Gondwanan margin (right hand side). The different perspective on the left-hand side illustrates the relationships between Laurentia, Baltica, Gondwana and the intervening Rheic and Iapetus oceans (from Domeier 2016, 2017). (B) Sketch map showing the distribution of the main tectonic elements of Iran. (**C**) Simplified map of the study area south of Fariman, with sample locations (from de Garmont et al. 1984).

Fig. 2: (A) Sheared dyke in Chahak granite: (B) Locally sheared gabbro. (C) Mineral assemblage in gabbro, with diopside locally surrounded by brown hornblende and partially retrogressed to actinolite along fractures. The light mineral is plagioclase. (D) Zoned and partially altered plagioclase crystal in granite. (E) Typical zircon morphology in granite. The more equant grains contain older components. (F) Appearance of the sparse zircons extracted from gabbro, few with euhedral shapes and most as fragments. The brown domains are U-rich and altered parts. The analyses were done on clear domains liberated by air abrasion. Grains in E and F are betweent 100 and 300 um long.

Fig. 3. (A) Plot of REE normalized to CI chondrite values of Sun and McDonough (1989) for the granite (thick lines) and the gabbro (thin lines; from Homam 2015)). (B) spider diagram for granite and gabbro compositions, normalized to primitive mantle values of Sun and McDonough (1989).

Fig. 4. Trace element discrimination diagrams for granite data (after Pearce et al. 1984); ORG = ocean ridge granites, VAG = volcanic arc granites, WPG = within plate granites, COLG = collision granites.

Fig. 5. Concordia diagrams with zircon U-Pb data for granite and gabbro. Ellipses indicate 2 sigma uncertainty.

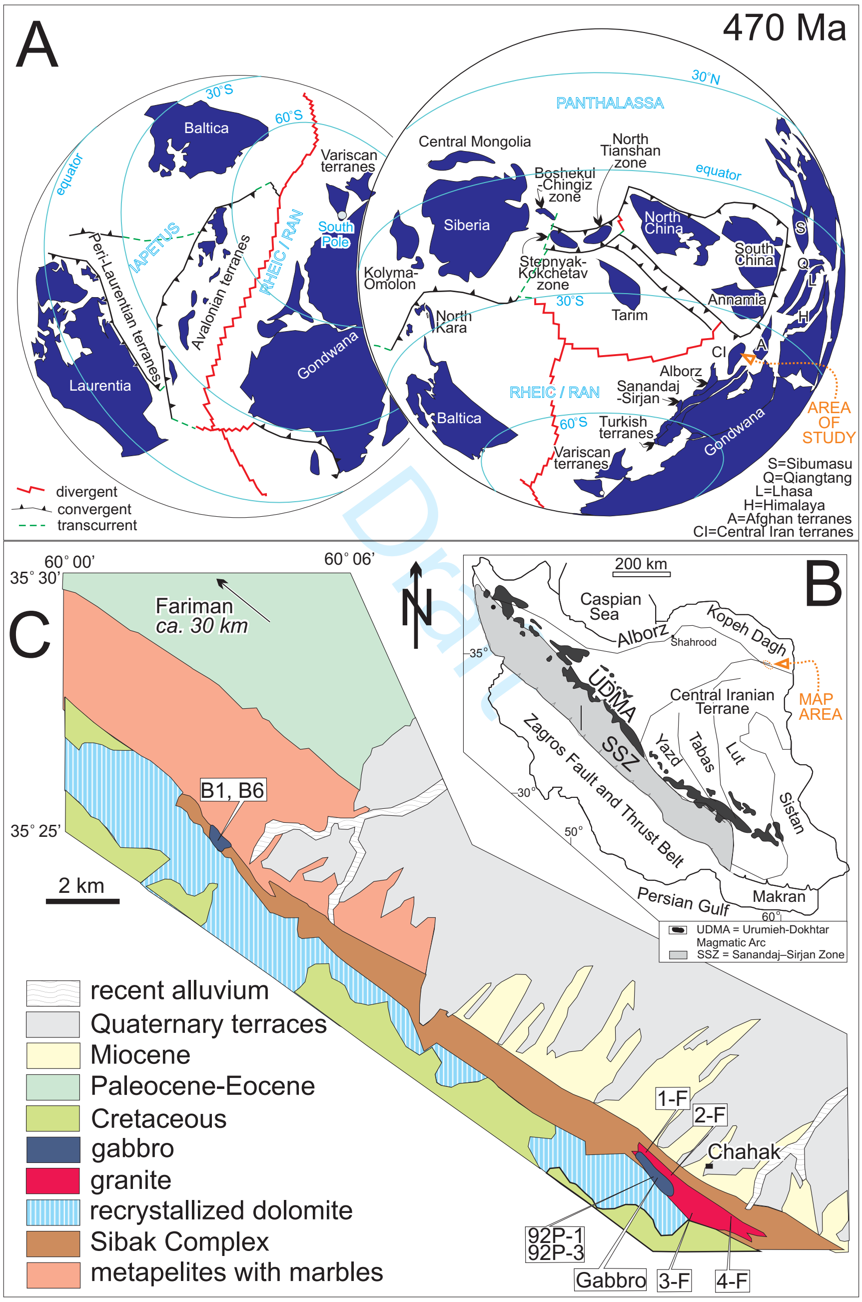
A
470 Ma
Baltica
Variscan terranes
Peri-Laurentian terranes
IAPETUS
Avalonian terranes
RHEIC / RAN
South Pole
Laurentia
Gondwana
PANTHALASSA
Central Mongolia
North Tianshan zone
Boshekul -Chingiz zone
Siberia
Kolyma-Omolon
Stepnyak-Kokchetav zone
North China
South China
Annamia
Tarim
North Kara
Alborz
Sanandaj -Sirjan
Turkish terranes
Variscan terranes
AREA OF STUDY
divergent
convergent
transcurrent
S=Sibumasu
Q=Qiangtang
L=Lhasa
H=Himalaya
A=Afghan terranes
CI=Central Iran terranes
B
200 km
Caspian Sea
Alborz
Kopeh Dagh
Shahrood
MAP AREA
Central Iranian Terrane
UDMA
SSZ
Yazd
Tabas
Lut
Sistan
Zagros Fault and Thrust Belt
Persian Gulf
Makran
UDMA = Urumieh-Dokhtar Magmatic Arc
SSZ = Sanandaj–Sirjan Zone
C
60° 00'
60° 06'
35° 30'
35° 25'
Fariman ca. 30 km
B1, B6
2 km
1-F
2-F
Chahak
92P-1
92P-3
Gabbro
3-F
4-F
recent alluvium
Quaternary terraces
Miocene
Paleocene-Eocene
Cretaceous
gabbro
granite
recrystallized dolomite
Sibak Complex
metapelites with marbles

Fig. 1

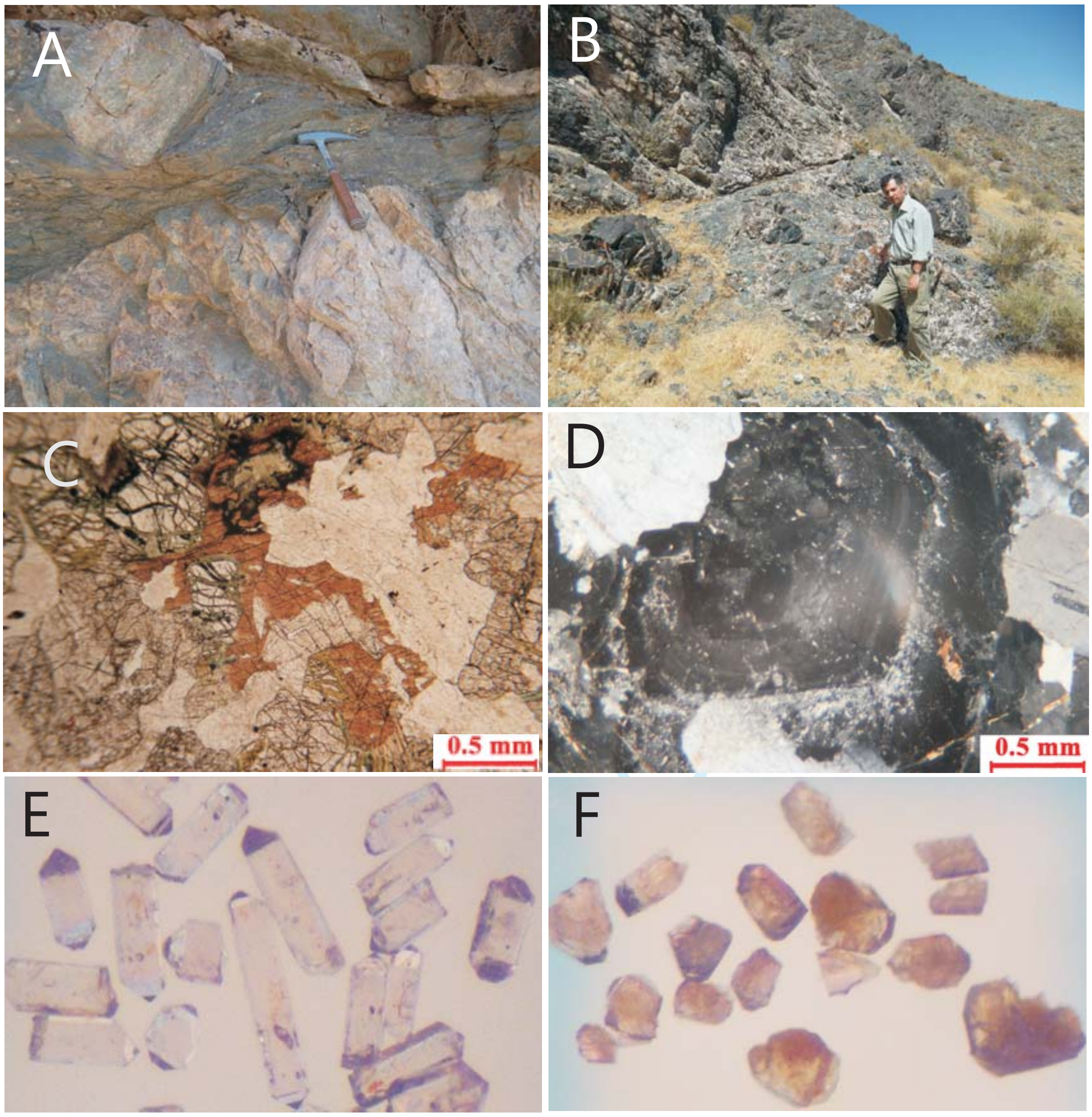

Fig. 2

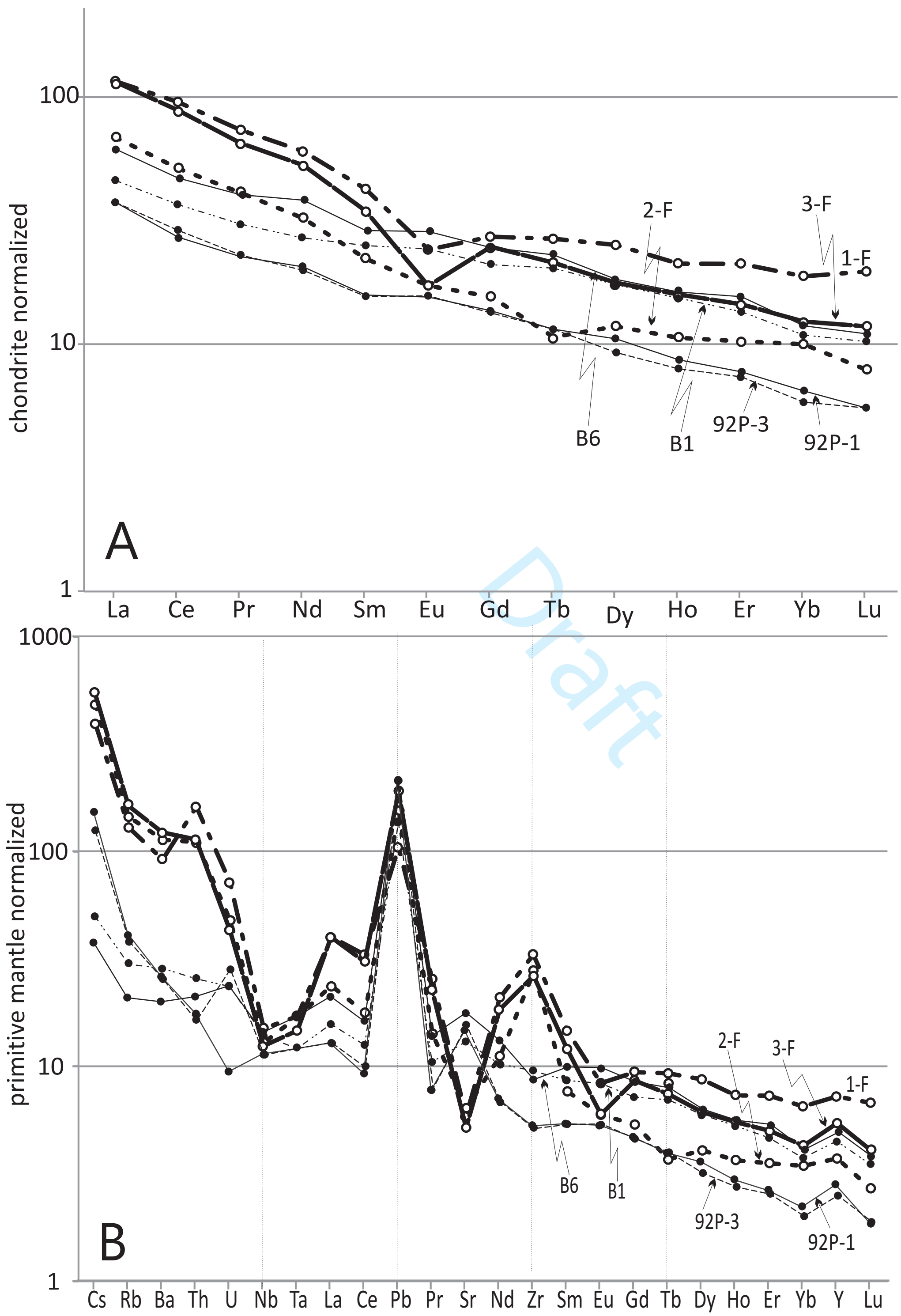
chondrite normalized
100
10
1
A
La Ce Pr Nd Sm Eu Gd Tb Dy Ho Er Yb Lu
2-F
3-F
1-F
B6
B1
92P-3
92P-1
primitive mantle normalized
1000
100
10
1
B
Cs Rb Ba Th U Nb Ta La Ce Pb Pr Sr Nd Zr Sm Eu Gd Tb Dy Ho Er Yb Y Lu
2-F
3-F
1-F
B6
B1
92P-3
92P-1

Fig. 3

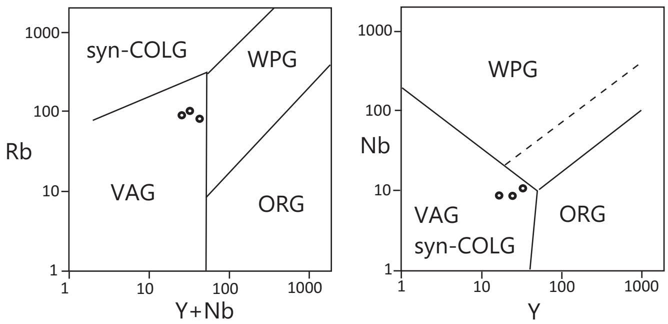
Rb
1000
100
10
1
1
10
100
1000
Y+Nb
syn-COLG
WPG
VAG
ORG
Nb
1000
100
10
1
1
10
100
1000
Y
WPG
VAG
syn-COLG
ORG

Fig. 4

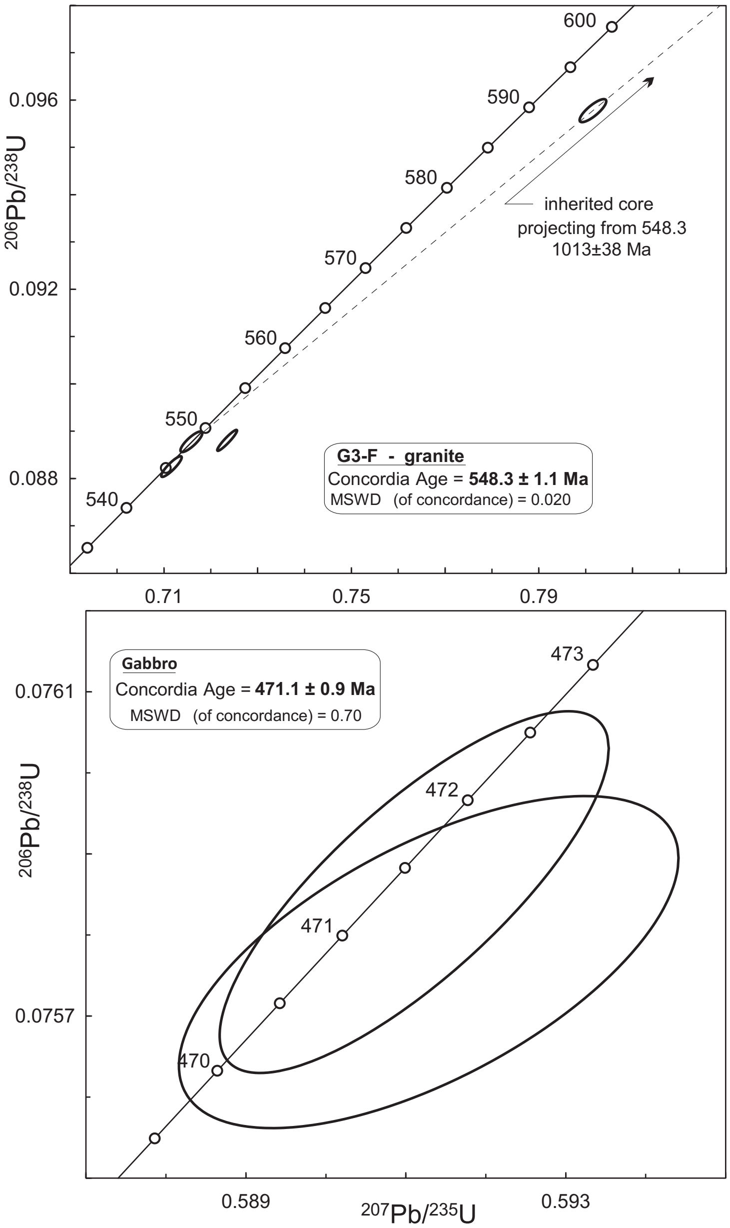
600
590
580
570
560
550
540
0.096
0.092
0.088
206Pb/238U
inherited core
projecting from 548.3
1013±38 Ma
G3-F - granite
Concordia Age = 548.3 ± 1.1 Ma
MSWD (of concordance) = 0.020
0.71
0.75
0.79
Gabbro
Concordia Age = 471.1 ± 0.9 Ma
MSWD (of concordance) = 0.70
473
472
471
470
0.0761
0.0757
206Pb/238U
0.589
0.593
207Pb/235U

Fig. 5

Table 1. Geochemical data for Chahak granite.

[%]	1-F	2-F	3-F	4-F
SiO_2	69.52	69.91	71.24	71.17
Al_2O_3	13.90	14.09	13.73	12.45
Fe_2O_3	5.37	4.80	4.45	4.05
MgO	0.89	0.79	0.66	0.51
CaO	1.60	1.40	0.96	1.24
K_2O	2.31	2.75	3.04	2.98
Na_2O	4.83	4.42	4.31	4.15
TiO_2	0.46	0.44	0.34	0.32
MnO	0.07	0.06	0.05	0.05
P_2O_5	0.09	0.08	0.07	0.07
LOI	0.68	0.86	0.85	2.74

[ppm]	1-F	2-F	3-F
Cs	3.10	3.80	4.30
Rb	82	92	103
Ba	640	793	853
Th	13.7	9.4	9.6
U	1.50	1.00	0.90
Nb	10.7	9.2	8.8
Ta	0.70	0.70	0.60
La	27.5	16.3	27.3
Ce	58.5	31.5	54.2
Pb	7.4	11.1	13.4
Pr	7.0	3.9	6.2
Sr	124	135	109
Nd	28.2	15.1	24.8
Zr	370	310	294
Sm	6.50	3.40	5.30
Eu	1.40	1.00	1.00
Gd	5.60	3.20	5.10
Tb	1.00	0.40	0.80

[ppm]	1-F	2-F	3-F
Dy	6.40	3.00	4.50
Ho	1.20	0.60	0.90
Er	3.50	1.70	2.40
Tm	0.6	0.3	0.3
Yb	3.20	1.70	2.10
Y	32.9	17.0	24.7
Lu	0.50	0.20	0.30
Li	18.9	28.9	26.2
Be	2.00	3.00	2.00
Ga	19.4	19.4	17.5
Ni	3.80	4.10	5.50
Zn	55.0	57.3	49.3
Cu	5.1	4.1	6.4
Mo	1.0	1.1	1.4
Co	4.3	4	3.5
Cr	24.0	23.0	29.0
Sn	2.80	2.10	2.40
Sc	11.40	7.70	8.60
S	<0.04	<0.04	<0.04
V	25.0	24.0	21.0
Cd	0.04	0.03	0.06
Sb	0.8	1.37	1.81
Bi	<0.04	0.06	<0.04
W	0.5	0.3	0.5
In	0.07	0.05	0.07
Re	0.008	<0.002	<0.002
Se	<0.3	<0.3	<0.3
Te	<0.05	<0.05	<0.05
Tl	0.38	0.43	0.48

Table 2. U-Pb data.

Properties (a)	Weight [ug] (b)	U [ppm] (b)	Th/U (c)	Pbc [pg] (d)	206/204 (e)	207/235 (f)	2 sigma [abs] (f)	206/238 (f, g)	2 sigma [abs] (f)	rho (f)	207/206 (f,g)	2 sigma [abs] (f)	206/238 [Ma] (f)	2 sigma [abs] (f)	207/235 [Ma] (f)	2 sigma [abs] (f)	206/207 [Ma] (f)	2 sigma [abs] (f)
G3-F - granite																		
Z eu tips CA [5]	4	262	0.47	0.4	13536	0.71161	0.00178	0.08825	0.00018	0.89	0.05848	0.00007	545.2	1.1	545.7	1.1	547.8	2.5
Z eu lp-fr CA [6]	6	384	0.45	1.5	8624	0.71586	0.00191	0.08878	0.00018	0.84	0.05848	0.00009	548.3	1.1	548.2	1.1	547.9	3.2
Z eu lp-fr CA [10]	24	360	0.49	1.3	36733	0.72349	0.00172	0.08881	0.00018	0.94	0.05909	0.00005	548.5	1.1	552.7	1.0	570.3	1.9
Z eu sp CA [1]	4	301	0.44	1.4	5027	0.80156	0.00233	0.09578	0.00020	0.81	0.06070	0.00010	589.6	1.2	597.7	1.3	628.6	3.7
Gabbro																		
Z eu fr pk AA [1]	1	1446	2.73	1.4	4813	0.59110	0.00199	0.07585	0.00018	0.79	0.05652	0.00012	471.3	1.1	471.6	1.3	472.8	4.6
Z eu fr pk AA [1]	1	671	1.66	1.6	1995	0.59129	0.00255	0.07577	0.00017	0.63	0.05660	0.00019	470.8	1.0	471.7	1.6	476.0	7.5

a) Z = zircon; eu = euhedral, lp = long prismatic; sp = short prismatic; fr = fragment; pk = pink; CA = zircon treated with chemical abrasion (Mattinson 2005), AA = zircon treated with air abrasion (Krogh 1982)

b) weight and concentrations are known to better than 10%.

c) Th/U model ratio inferred from 208/206 ratio and age of sample

d) Pbi = initiall Pb (corrected for blank); Pbc = total common Pb in sample (initial + blank)

e) raw data, corrected for fractionation and spike

f) corrected for fractionation, spike and blank (206/204=18.59; 207/204=15.24); error calculated by propagating the main sources of uncertainty; The U-Pb ratio of the spike used for this work is adapted to 206Pb/238U = 0.015660 for the ET100 solution as obtained with the ET2535 spike at NIGL.

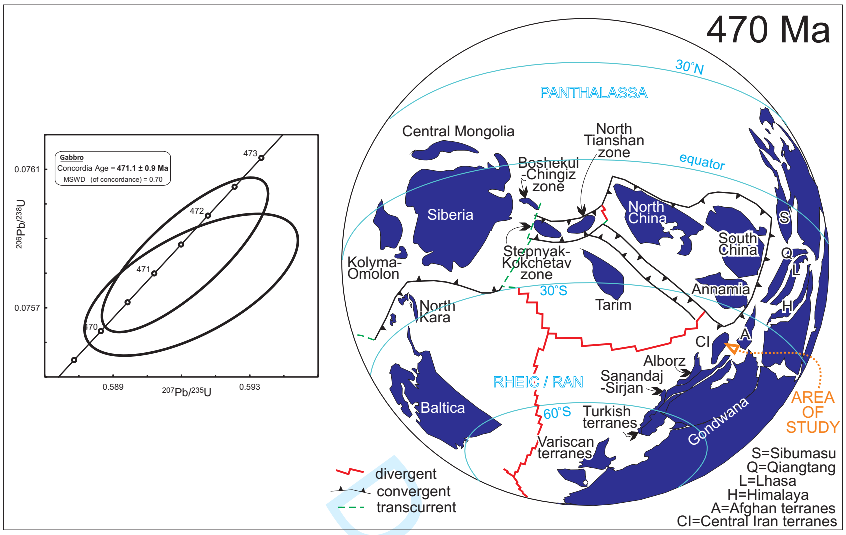
Gabbro
Concordia Age = 471.1 ± 0.9 Ma
MSWD (of concordance) = 0.70
473
472
471
470
0.0761
0.0757
$^{206}Pb/^{238}U$
0.589
0.593
$^{207}Pb/^{235}U$
470 Ma
30°N
PANTHALASSA
equator
Central Mongolia
North Tianshan zone
Boshekul -Chingiz zone
Siberia
Stepnyak- Kokchetav zone
North China
South China
Kolyma- Omolon
North Kara
30°S
Tarim
Annamia
S
Q
L
H
A
CI
Alborz
Sanandaj -Sirjan
RHEIC / RAN
Baltica
60°S
Turkish terranes
Variscan terranes
Gondwana
AREA OF STUDY
divergent
convergent
transcurrent
S=Sibumasu
Q=Qiangtang
L=Lhasa
H=Himalaya
A=Afghan terranes
CI=Central Iran terranes